Active Cloaking and Illusion of Electric Potentials in Electrostatics

Andreas Helfrich-Schkabarenko
Esslingen University of Applied Sciences
Alik Ismail-Zadeh (alik.ismail-zadeh@kit.edu)
Karlsruhe Institute of Technology, Institute of Applied Geosciences, Karlsruhe, Germany;
Aron Sommer
University of Hannover

Research Article

Keywords: cloaking, self-potentials, inverse theory, numerical modelling, numerical solutions, electric properties

Posted Date: January 7th, 2021

DOI: https://doi.org/10.21203/rs.3.rs-140026/v1

ACTIVE CLOAKING AND ILLUSION OF ELECTRIC POTENTIALS IN ELECTROSTATICS

Andreas Helfrich-Schkabarenko[1], Alik Ismail-Zadeh[2,3], Aron Sommer[4]

[1] *University of Applied Sciences, Esslingen, Germany;*
Andreas.Helfrich-Schkarbanenko@hs-esslingen.de
[2] *Karlsruhe Institute of Technology, Institute of Applied Geosciences, Karlsruhe, Germany;*
Alik.Ismail-Zadeh@kit.edu
[3] *Russian Academy of Sciences, Institute of Earthquake Prediction Theory and Mathematical Geophysics, Moscow, Russia; aismail@mitp.ru*
[4] *Leibniz University Hannover, Institute of Information Processing, Hannover, Germany;*
sommer@tnt.uni-hannover.de

Summary - Cloaking and illusion has been demonstrated theoretically and experimentally in several research fields. Here we present for the first time an active exterior cloaking device in electrostatics operating in a two-horizontally-layered electroconductive domain, and use the superposition principle to cloak electric potentials. The device uses an additional current source pattern introduced on the interface between two layers to cancel the total electric potential to be measured. Also, we present an active exterior illusion device allowing for detection of a signal pattern corresponding to any arbitrarily chosen current source instead of the existing current source. The performance of the cloaking/illusion devices is demonstrated by three-dimensional models and numerical experiments using synthetic measurements of the electric potential. Sensitivities of numerical results to a noise in measured data and to a size of cloaking devices are analysed. The numerical results show quite reasonable cloaking/illusion performance, which means that a current source can be hidden electrostatically. The developed active cloaking/illusion methodology can be used in subsurface geo-exploration studies, electrical engineering, live sciences, and elsewhere.

Short title: Cloaking and illusion in electrostatics

Key words: cloaking, self-potentials, inverse theory, numerical modelling, numerical solutions, electric properties

INTRODUCTION

Invisibility has been a subject of human fascination for millennia. The basic idea of invisibility is to generate a cloaking device and use it to hide an object. Cloaking devices employ specially designed structures that would make objects 'invisible' by detecting devices (e.g. eyes, antennas, airborne or satellite detectors/sensors). Over the last two decades, theoretical and experimental studies on cloaking have been conducted in several research fields such as electromagnetism [1,2,3], acoustics [4,5,6], thermodynamics [7,8,9,10], solid mechanics [11], elastic [12, 13, 14, 15], and seismic wave propagation [16, 17, 18, 19].

Cloaking devices can differ by its construction (*interior* and *exterior cloaking*) and by transforming physical properties of the material surrounding an object (*passive cloaking*) or adding an active source (*active cloaking*). An *interior cloaking device* surrounds an object to be cloaked, so that, the object is located in the interior of the cloaking device [1]. An *exterior cloaking device* hides objects from potential detections without encompassing them [20]. A *passive* cloaking device induces invisibility by a special choice of physical parameters of a designed artificial material (so-called *metamaterial*) surrounding or partly surrounding an object, so that, an incident wave on the object bypasses it without distortions. A mathematical technique used to develop metamaterials is transformation optics [21,22,23,24,25]. In the case of electrostatics, such metamaterial would be a material with an anisotropic electrical conductivity [26]. An *active cloaking* masks emitting objects using active sources [3,27,28,29].

In this paper, in horizontally-layered electroconductive domain we use active exterior cloaking devices in the case of electrostatics to mask current source located in the source sub-domain (SSD), e.g. Earth's ground, so making the source nearly undetectable by measurements in the observational sub-domain (OSD), e.g., seawater (Fig. 1). An "invisibility" in this case is achieved by using the current source networks suitably constructed on the interface between the two sub-domains (hereinafter referred to as ISD), which cancel (cloak) or generate imaginary (illusion) electric potential in the OSD. A mathematical background for developing the active cloaking devices lies in the theory of inverse problems [30] with the use of the superposition principle in terms of active noise control or noise cancellation [31,32]. In a three-dimensional model domain comprised of two overlain electroconductive layers, the following direct and inverse problems form essential components of our numerical experiments based

on an electrostatic model.

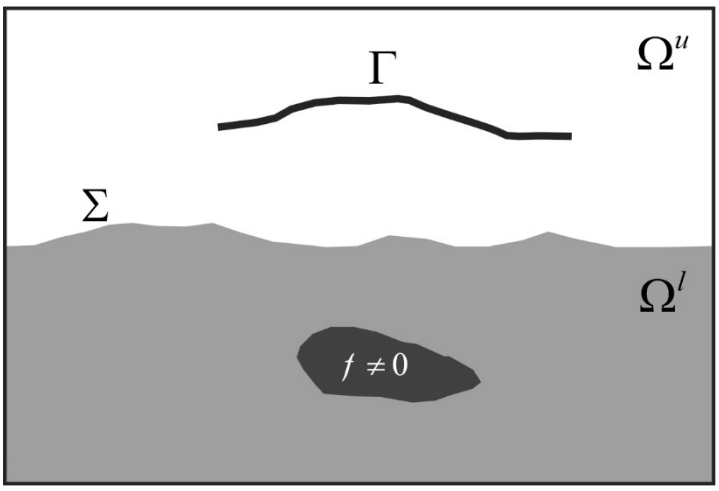

Figure **1**. Two-dimensional cartoon of the model domain Ω. Dark gray: the area of non-zero current source density; light gray: the SSD Ω^l; Σ is the ISD; Ω^u is the OSD; and Γ is a curve (or a set) of measurement points.

- *Direct Problem*: To find the generated electrical potential in the entire model domain for a given non-zero current source density located in SSD.
- *Source Identification Problem*: To determine this current source density from its electric potential, which can be measured or inferred from measured electromagnetic data in the OSD. As the source identification problem was analysed by Sommer et al. (ref. [33]), here we describe briefly the results of this study. Applications of the source identification problem are numerous; for example, it is the subject of research in volcanology [34,35] and in geo-explorations [36].
- *Active Cloaking Problem*: To cloak the current source density so that it gets 'invisible' for measurements in the OSD. To achieve it, we introduce an additional current source density (thereafter referred to as *active cloaking device*) on the ISD in order to minimize the total electric potential field in the OSD.
- *Active Illusion Problem:* To generate an illusion in the data measured in the OSD by manipulating the total electric potential field. The manipulation is set up via an additional current source density on the ISD. A similar approach was used in electromagnetics [37]. Essentially, an active illusion problem is based on an active cloaking problem.

In what comes next, we present results of the four interconnected problems mentioned above. Synthetic data (that is, an electric potential) are generated by solving the direct problem (hereinafter we refer to the synthetic data as "measured" data). These data are employed as the input data in the source identification problem to determine the current source density. The active cloaking and illusion devices are then introduced to mask the current source, and the effectiveness of the devices is demonstrated.

RESULTS

Electric potential determination

The electric potential u (measured in V) is determined from the volumetric current source density $f \neq 0$ (also known as the self-potential source [38,39]) by solving the boundary value problem for the conductivity equation

$$-\nabla \cdot (\sigma(\mathbf{x}) \nabla u(\mathbf{x})) = f(\mathbf{x}), \quad \mathbf{x} \in \Omega \tag{1}$$

with the Robin condition at the boundary of the model domain [40]

$$\sigma(\mathbf{x}) \frac{\partial u(\mathbf{x})}{\partial \mathbf{n}(\mathbf{x})} + g(\mathbf{x}) u(\mathbf{x}) = 0, \quad \mathbf{x} \in \partial\Omega. \tag{2}$$

Here σ is the electrical conductivity (measured in $\mathrm{S\ m^{-1}}$); $\mathbf{x} = (x_1, x_2, x_3)^T$ are the Cartesian coordinates; $\Omega = \Omega^l \cup \Sigma \cup \Omega^u \subset \mathbb{R}^3$ is the three-dimensional model domain (its description can be found in *Method*, and its two-dimensional sketch in Fig. 1); Ω^l is the SSD, Ω^u is the OSD, Σ is the ISD; $\mathbf{n}$ is the outward unit normal vector at a point on the boundary $\partial\Omega$, which restricts $\mathbb{R}^3$ to a bounded domain Ω; and g is a non-negative function defined at the model boundary as the reciprocal distance from the boundary to the geometrical centre of the model domain Ω.

To solve the problem (1)-(2) numerically, the finite-element method is used [41,42]. The solution to a discrete problem corresponding to the weak formulation of the problem (1)-(2) can be presented as:

$$\mathbf{u} = \mathbf{A}\mathbf{f}, \tag{3}$$

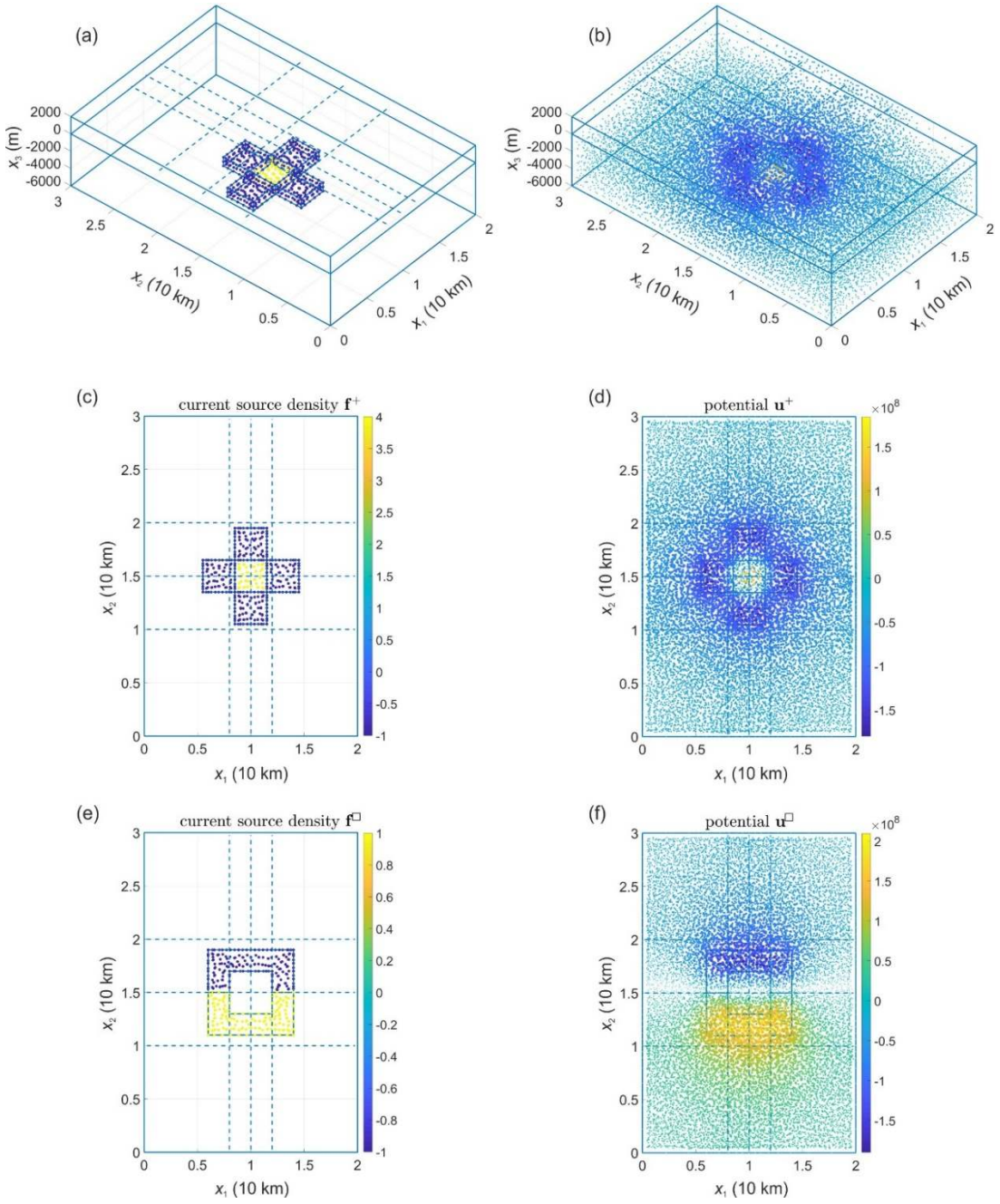

Figure 2. Electric potentials generated by two current source densities. The perspective view (a) and top view (c) of the current source density $\mathbf{f}^+$; the perspective view (b) and top view (d) of the electric potential $\mathbf{u}^+$ generated by the current source density. Top view of the electric potential $\mathbf{u}^\square$ (f) generated by $\mathbf{f}^\square$ (e). Here and in Figs. 3-6, a top view image presents a transparent projection of physical quantities at finite element nodes on the plane. The size of the nodes in the images is proportional to the absolute value of the physical quantities it represents, i.e. the nodes with zero-values are not displayed. Dashed lines show the position of the paths, along which synthetic measurements of the electric potential have been made.

where **u** and **f** are the discrete representations of the electric potential and the current source density, respectively, and **A** is the solver operator (see *Method*). The solutions $\mathbf{u}^{+}$ and $\mathbf{u}^{\square}$ for two different current source densities $\mathbf{f}^{+}$ and $\mathbf{f}^{\square}$, respectively (see *Method* for description of the current source densities), are illustrated in Fig. 2. As measurements of the electric potential are restricted to a part of Ω^{u} (OSD), we introduce the restriction operator $\mathbf{T}$, which restricts $\mathbf{u}$ to the measured data $\mathbf{u}_d := \mathbf{T}\mathbf{u} := \mathbf{u}\big|_{\Gamma}$, where $\Gamma \subset \Omega^{u}$ is a curve or a set of measurement points. Using equation (3), we obtain:

$$\mathbf{u}_d = \mathbf{T}\mathbf{A}\,\mathbf{f} =: \mathbf{A}_d\mathbf{f}\,. \tag{4}$$

Current source identification

The current source density $\mathbf{f}$ can be formally determined from the measurements of the electric potential $\mathbf{u}_d$ by solving equation (4), namely, $\mathbf{f} = \mathbf{A}_d^{-1}\mathbf{u}_d$. Meanwhile, it is shown that a solution of this inverse problem exists, but it is not unique [33]. A Tikhonov regularization can enforce the uniqueness of a solution via a spectral shift by using the operator $\mathbf{A}_d{}^{\mathrm{T}}\mathbf{A}_d$, where $\mathbf{A}_d^{\mathrm{T}}$ is the transpose of operator $\mathbf{A}_d$ [30,43]. Doing so, the following solution to the regularized inverse problem for given measurements $\mathbf{u}_d$ can be obtained:

$$\mathbf{f}_\alpha := \mathbf{\Lambda}_\alpha\mathbf{u}_d, \qquad \mathbf{\Lambda}_\alpha = (\mathbf{A}_d^{\mathrm{T}}\mathbf{A}_d + \alpha\mathbf{D}^{\mathrm{T}}\mathbf{D})^{-1}\mathbf{A}_d^{\mathrm{T}}, \tag{5}$$

where $\alpha > 0$ is the regularization parameter, and $\mathbf{D}^{T}\mathbf{D}$ is the penalty term corresponding to the Nabla (∇) operator. As the choice of α is a critical point in the Tikhonov regularization method, we apply the *L*-curve criterion to find the optimal value of the regularization parameter [44].

The inverse problem (equation 5) is solved numerically using the same current source densities $\mathbf{f}^{+}$ and $\mathbf{f}^{\square}$. It is assumed that Γ consists of a set of 300 points located in the OSD along three lines at the height of 500 m (parallel to x_1-axis) and three lines at the height of 1000 m (parallel to x_2-axis) above the plane x_3=0 (Fig. 3 a, c). The data determined on Γ are used to reconstruct $\mathbf{f}_\alpha^{+}$ and $\mathbf{f}_\alpha^{\square}$ as shown in equation (5), and the inversion's results are shown in Fig. 3b, d. The performance of regularization and the sensitivity of the numerical results have been tested by introducing a random noise on measurements $\mathbf{u}_d$. It is shown that the quality of the reconstructions of the current source density decreases with the noise (see *Supplementary*

Material; Fig. S1).

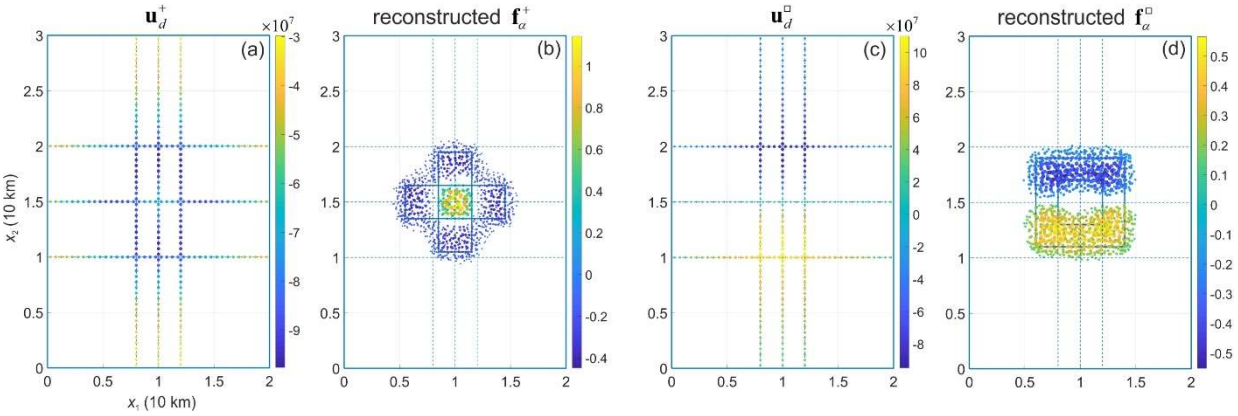

Figure 3. Electric potential $\mathbf{u}_d^+$ (a) and $\mathbf{u}_d^\square$ (c) along the paths of synthetic measurements, and the current source density $\mathbf{f}_\alpha^+$ (b) and $\mathbf{f}_\alpha^\square$ (d) reconstructed from the synthetic measured data.

Active cloaking

To cloak an electric current source in the SSD, we design an active cloaking device introducing a complementary electric current source density $\mathbf{f}_c$, so that $\mathbf{f}+\mathbf{f}_c \neq 0$, and using the superposition principle. As the inverse problem associated with the active cloaking device is linear, the superposition principle can be applied. In doing so, the total electrical potential field vanishes on Γ (measurement paths), reduces in the OSD significantly, and hence becomes almost undetectable by measurements. Applying the operator $\mathbf{A}_d$ to the combined electric current source density, we obtain

$$\mathbf{A}_d\left(\mathbf{f}+\mathbf{f}_c\right)=\mathbf{A}_d\mathbf{f}+\mathbf{A}_d\mathbf{f}_c=\mathbf{u}_d+\mathbf{A}_d\mathbf{f}_c=0, \tag{6}$$

i.e. $\mathbf{A}_d\mathbf{f}_c=-\mathbf{u}_d$. The cloaking procedure is described as

$$\mathbf{u}_d \overset{-\Lambda_{c,\alpha}}{\mapsto} \mathbf{f}_{c,\alpha} \overset{\mathbf{A}_{d,c}}{\mapsto} \mathbf{u}_{d,c}\approx-\mathbf{u}_d, \tag{7}$$

and hence $(\mathbf{f}+\mathbf{f}_{c,\alpha}) \overset{\mathbf{A}_d}{\mapsto} (\mathbf{u}_d+\mathbf{u}_{d,c})\approx 0$ on Γ. Here $\Lambda_{c,\alpha}$ is the cloaking operator; $\mathbf{f}_{c,\alpha}$ is the current source density of the cloaking device; $\mathbf{A}_{d,c}$ is the adapted operator, which maps the cloaking current source density $\mathbf{f}_{c,\alpha}$ to electrical potential $\mathbf{u}_{d,c}$ on Γ; and the notation $\mathbf{w} \overset{\Phi}{\mapsto} \mathbf{h}$ means $\mathbf{\Phi w}=\mathbf{h}$ (see *Method* for detail).

In numerical experiments, we consider the current source densities $\mathbf{f}^{+}$ and $\mathbf{f}^{\square}$ and apply the cloaking operator $\mathbf{\Lambda}_{c,\alpha}$ to synthetic data $\mathbf{u}_d^{+}$ and $\mathbf{u}_d^{\square}$. The cloaking current pattern $\mathbf{f}_{c,\alpha}^{+}$ and $\mathbf{f}_{c,\alpha}^{\square}$ are presented in Figs. 4 and 5, respectively. Comparing the images of $\mathbf{A}_d\mathbf{f}^{+}$ (Fig. 4a) and $\mathbf{A}_{d,c}\mathbf{f}_{c,\alpha}^{+}$ (Fig. 4c), we see that the images are almost identical up to their sign, and their sum is almost vanishing (Fig. 4d). The cloaking operator $\mathbf{\Lambda}_{c,\alpha}$ significantly reduces the amplitude of the total electric potential from about 10^8 to 10^2 V (Fig. 4b,e). Similarly, the operator $\mathbf{\Lambda}_{c,\alpha}$ reduces the amplitude of the total electric potential in the case of the current source $\mathbf{f}^{\square}$ (Fig. 5). Figures 4e and 5e illustrate the cancellation of the signals $\mathbf{u}_d^{+}+\mathbf{u}_{d,c}^{+}$ and $\mathbf{u}_d^{\square}+\mathbf{u}_{d,c}^{\square}$, respectively, where the dashed line represents the total electric potential field. The cloak regime masks the source for measurements, and, therefore, the current source becomes invisible electrostatically, i.e. cloaked. Note that the cloaking device (i.e. electric current source density $\mathbf{f}_{c,\alpha}$; Figs. 4*b* and 5*b*) was designed based on data $\mathbf{u}_d$ and not on $\mathbf{f}$.

In the numerical experiments presented here, the position and size of the cloaking device on the ISD have been fixed. To what extent do its position and size affect the cloaking? To answer the questions, we have performed several numerical experiments (see *Supplementary Materials)*. It is shown that the accuracy of the devices enhances with the increasing size of the devices (Fig. S2). A shift of the cloaking devices may improve the quality of invisibility (Figs. S3 and S4). Hence, a search for the optimal size and the position of a cloaking device will assist in enhancing invisibility.

When developing the cloaking device, we have considered synthetic data of the electric potential along several paths in the OSD, i.e. the cloaking device ensures that the electric potential becomes insignificant (invisible) on the paths. Meanwhile, how would the cloaking device look like and how effective would it be, if we use not only these paths to develop the cloaking device, but the entire OSD? To ensure the invisibility of the current source everywhere in the OSD (not only along the paths of measurements), a cloaking device has been developed based on the measurements in the entire OSD. It is shown that although the quality of the cloaking lowers in this case, but still reducing the signal of electric potential by an order of magnitude (Fig. S5).

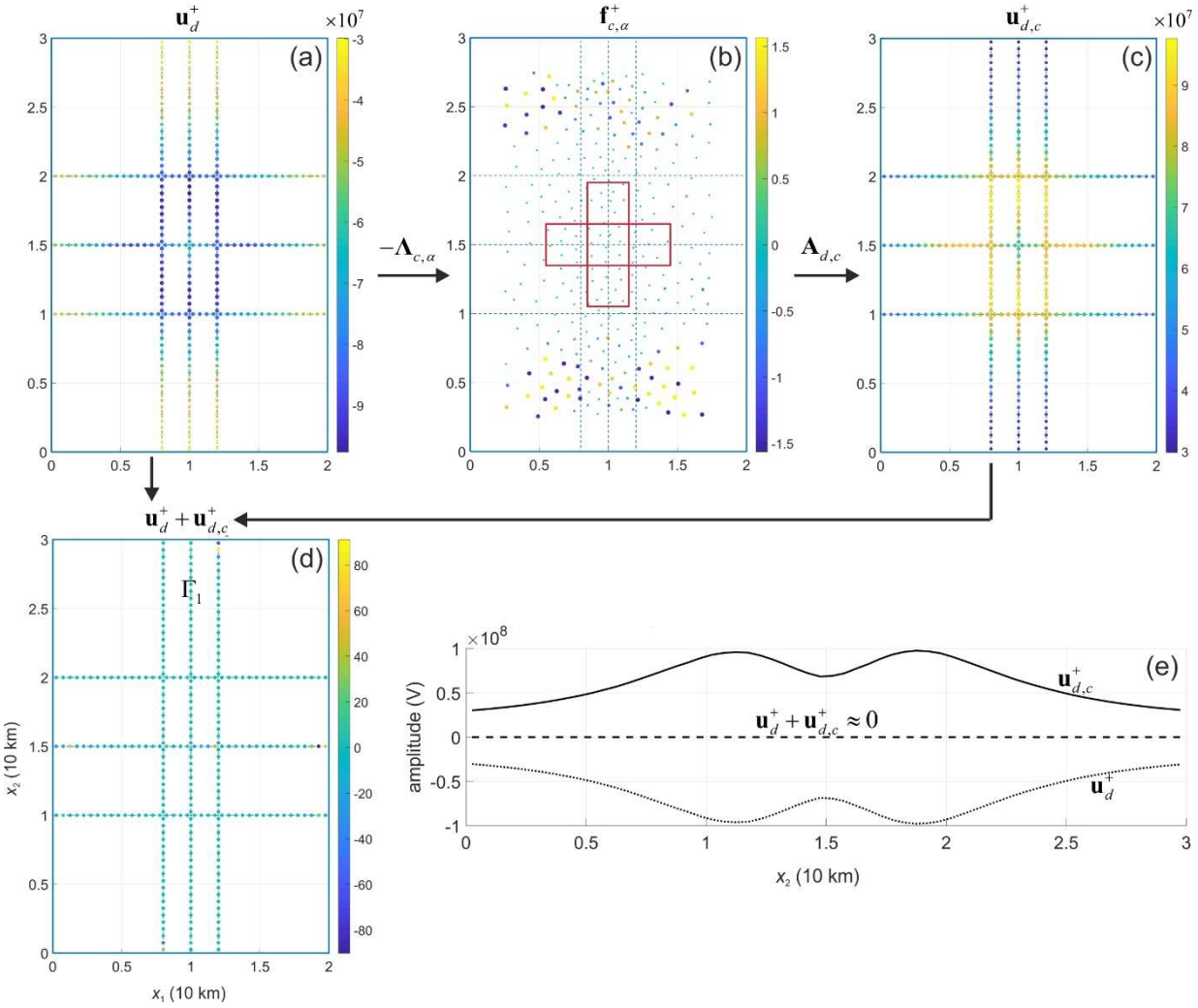

Fig. 4. Active cloaking of the electric potential $\mathbf{u}_d^+$ on Γ (a) generated by the current source density $\mathbf{f}^+$. Using equation (13) the cloaking devise is modelled by the current source density $\mathbf{f}_{c,\alpha}^+$ (b) that generates $\mathbf{u}_{d,c}^+$ (c) leading to a significant reduction (almost cancellation) of the electric potential signal on Γ (d). Panel (e) demonstrates the cancellation of the signal $\mathbf{u}_d^+ + \mathbf{u}_{d,c}^+$ (see dashed line) on the middle path (line Γ_1: $\{\mathbf{x} \in \Omega^u : x_1 = 0 \text{ km};\ x_3 = 0.5 \text{ km}\} \subset \Gamma$) of the synthetic measurement data.

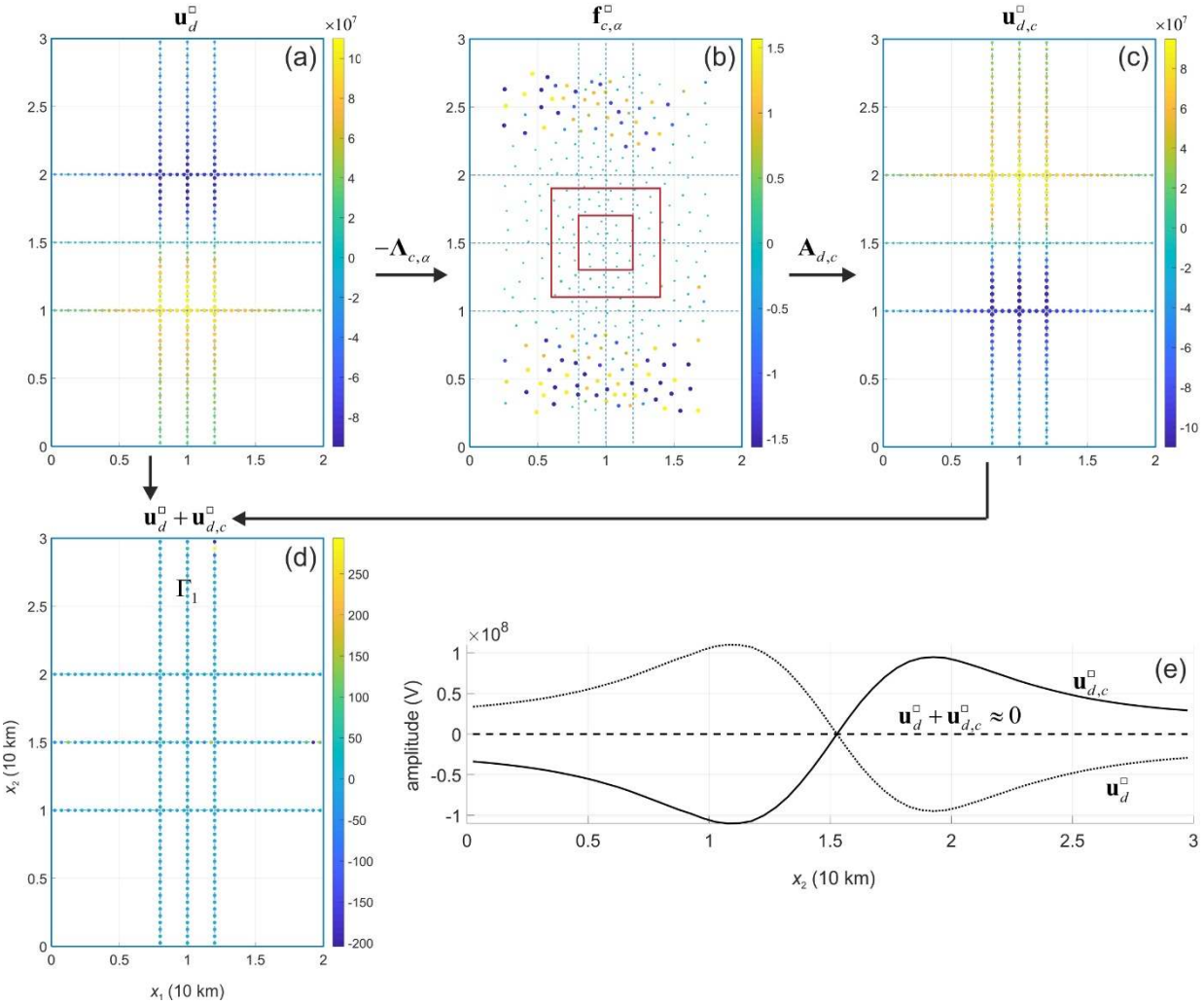

Fig. 5. Active cloaking of the electric self-potential $\mathbf{u}_d^{\square}$ on Γ (a) generated by the current source density $\mathbf{f}^{\square}$. Using equation (13) the cloaking devise is modelled by the current source density $\mathbf{f}_{c,\alpha}^{\square}$ (b) that generates $\mathbf{u}_{d,c}^{\square}$ (c) leading to a significant reduction (almost cancellation) of the electric potential signal on Γ (d). Panel (e) demonstrates the cancellation of the signal $\mathbf{u}_d^{\square}+\mathbf{u}_{d,c}^{\square}$ (see dashed line) on line Γ_1 $\{\mathbf{x}\in\Omega^a : x_1 = 0 \text{ km};\ x_3 = 0.5 \text{ km}\}\subset\Gamma$.

Active illusion

An illusion is generated in numerical experiments such a way that measurements in the OSD "detect" a current source artificially constructed instead of the existing current source located in the SSD. We achieve this by introducing a specially-designed illusion device, which, according to the principle of superposition, changes the total electric potential field in Ω^u into that generated by the current source density chosen for the illusion.

For given $\mathbf{f}^+$ in the SSD, we determine an additional current source density $\mathbf{f}_i = \mathbf{f}_c^+ - \mathbf{f}_c^{\square}$

on the ISD so that the inverse problem approach applied to the new data $\mathbf{u}_d^+ + \mathbf{A}_d\mathbf{f}_i$ delivers a solution corresponding to $\mathbf{f}_\alpha^\square$. Namely,

$$\mathbf{A}_d(\mathbf{f}^+ + \mathbf{f}_i) = \mathbf{A}_d(\mathbf{f}^+ + \mathbf{f}_c^+ - \mathbf{f}_c^\square) = \mathbf{A}_d\mathbf{f}^+ + \mathbf{A}_d\mathbf{f}_c^+ - \mathbf{A}_d\mathbf{f}_c^\square$$

$$= \underbrace{\mathbf{u}_d^+ + \mathbf{u}_{d,c}^+}_{\substack{\approx 0 \text{ (Eq. 13} \\ \text{in } \textit{Method}\text{)}}} - \mathbf{u}_{d,c}^\square \approx -\mathbf{u}_{d,c}^\square = -\mathbf{A}_d\mathbf{f}_c^\square \approx \mathbf{u}_d^\square. \qquad (8)$$

This means that the illusion pattern $\mathbf{f}_i$ generates "measured" data $\mathbf{u}_d^\square$ corresponding to $\mathbf{f}^\square$. The current source density $\mathbf{f}^\square$ has been chosen just for simplicity of the illustration of the illusion's results; any admissible current source density can be considered as an additional source.

The illusion procedure can be briefly described as $(\mathbf{f}^+ + \mathbf{f}_{c,\alpha}^+ - \mathbf{f}_{c,\alpha}^\square) \overset{\mathbf{A}_d}{\mapsto} \mathbf{u}_d \approx \mathbf{u}_d^\square$, where the cloaking patterns $\mathbf{f}_{c,\alpha}^+$ and $\mathbf{f}_{c,\alpha}^\square$ are determined from data $\mathbf{u}_d^+$ and $\mathbf{u}_d^\square$. Assuming that the given current source density is $\mathbf{f}^+$ (Fig. 6a), the cloaking pattern $\mathbf{f}_{c,\alpha}^+$ (Figs. 6b) and $\mathbf{f}_{c,\alpha}^\square$ (Figs. 6c) are computed. Then the operator $\mathbf{A}_d$ (equation 8) is applied to the current source density $\mathbf{f}^+ + \mathbf{f}_{c,\alpha}^+ - \mathbf{f}_{c,\alpha}^\square$ to get the resulting "measured" data $\mathbf{u}_d^\square$ (Fig. 6d). Finally, applying the cloaking operator $\mathbf{\Lambda}_{c,\alpha}$ the illusive current source density $\mathbf{f}_\alpha^\square$ is obtained (Fig. 6e).

DISCUSSION

In this work, an approach to design exterior active cloaking devices for self-potentials is presented, and it has been applied to an electrostatic problem so that an electric current source located in the SSD becomes "undetectable" by measurements in the OSD. Using synthetic examples of electric current sources, we have obtained that a constructed camouflage on the ISD allows to reduce significantly (at least by six orders of magnitude) the signal of the electrical self-potential on given measurement paths in the OSD, which is emanated from the electric current source located in the SSD. We note that the same approach can be applied to develop interior active cloaking devices by specifying the support of $\mathbf{f}_c$ around the source to be hidden, i.e., the cloaking device envelops the source completely.

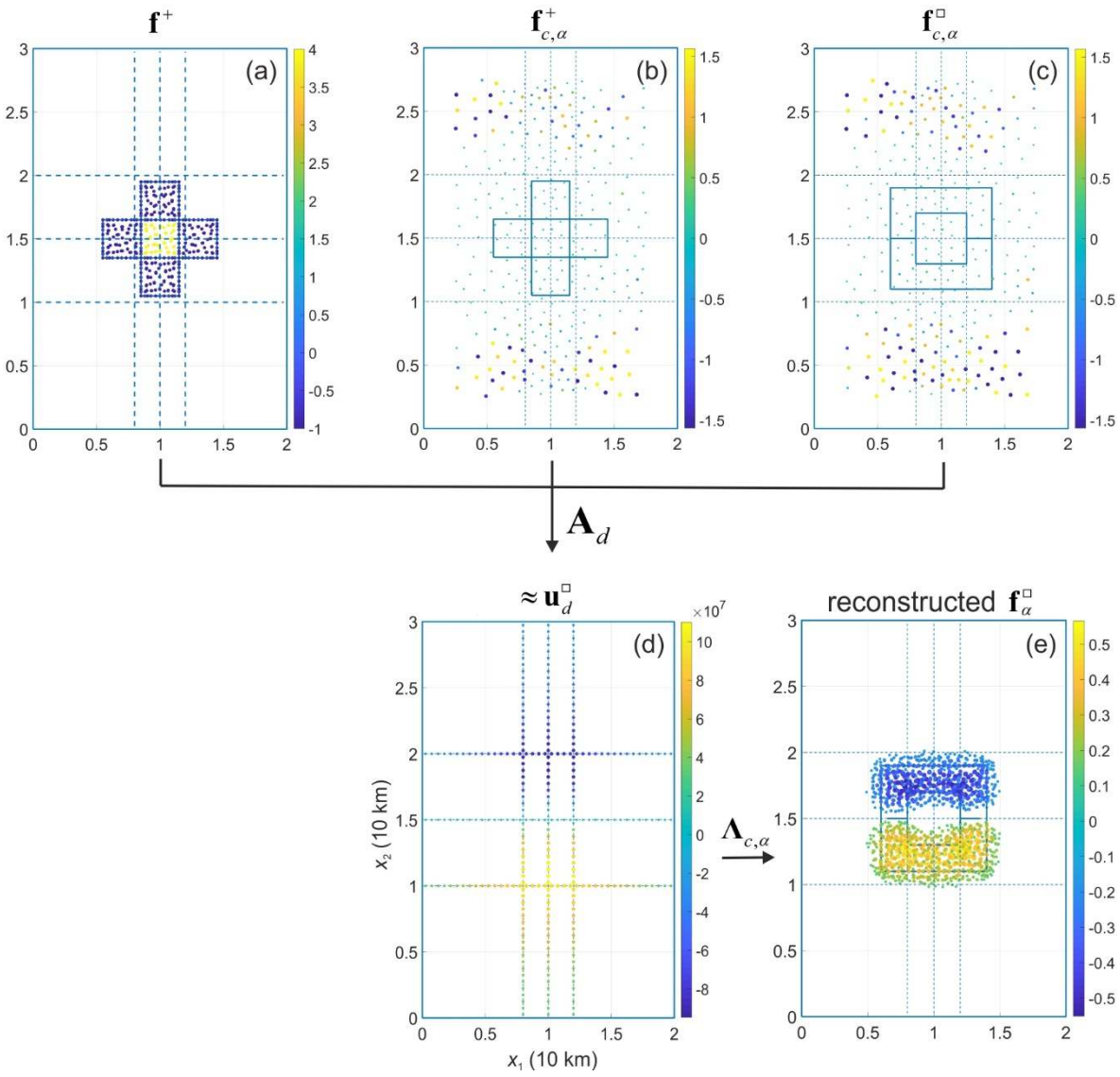

Fig. 6. Illusion of the current source density $\mathbf{f}^{\square}$ by cloaking of the current source density $\mathbf{f}^{+}$ (a) using cloaking devices $\mathbf{f}^{+}_{c,\alpha}$ (b) and $\mathbf{f}^{\square}_{c,\alpha}$ (c). Panel (d) represents a composition data on electric potential, which will be measured in the case of illusion (equation 16), and panel (e) illustrates the reconstruction of current source density from these measured data.

In addition, we have extended the idea of cloaking in electrostatic problems to illusion by manipulating the cloaking device so that the observed field of electric self-potential contains a superposition of hidden field created by the electric source in the SSD and a completely new field, which can be generated arbitrarily. Using synthetic examples, we have demonstrated the applicability of the illusion approach to the same electrostatic problem and shown that a

"cross"-type source in the SSD becomes invisible, but instead a "ring"-type source can be reconstructed from measurements in the OSD. Since it is more difficult to make an object completely invisible/undetectable due to the measurement inaccuracy and noise, an illusion device can help to hide a real shape of the source or object by mimicking another modelled shape. For example, a source or object could become smaller or bigger for an observer, like a transformation of the ogre into a lion and a mouse in the fairy tale *Puss in Boots* by Charles Perrault.

Electric self-potentials are usually generated by a number of natural sources, such as electrochemical, electrokinetic, thermoelectric, and mineral sources, as well as by a conducting fluid flow through the rocks. Self-potentials can fluctuate in the Earth with time due to different processes, e.g., alternating currents induced by effects of thunderstorms or heavy rainfalls; variations in Earth's magnetic fields [45]. As hydrocarbons in a reservoir are moving continuously because of stress and pressure differences, seismic or other vibrations, they create alterations in the electric potentials acting as an electric dipole in the geo-electromagnetic field [46,47].

Non-invasive measurements of self-potential in the subsurface does not require electric currents to be injected into the ground as in the cases of resistivity or induced polarisation tomography. The method has been used in geological explorations [48] to detect massive ore bodies, in groundwater and geothermal investigations, environmental and engineering applications, to monitor a salt plume, volcano and lava dome activities, and to reveal a borehole leak during hydraulic fracturing [49,50,51]. Airborne or seaborne geophysical surveying allows for detecting changes in physical variables of sub-surface processes in the Earth, e.g., in the electromagnetic potential and electric conductivity [52]. The surveying has been used for subsurface exploration, such as hydrocarbon exploration, groundwater management, and shallow drilling hazards.

The presented methods of cloaking and illusion can be used in geo-exploration. For example, depending on a commercial confidentiality, operators may wish to cloak the subsurface objects in electrostatic sense from airborne/seaborne measurements by other operators. We note that when the OSD is filled by seawater, an electric potential can be measured by seaborne surveys. Meanwhile, during airborne prospecting, a measured value is the amplitude of the magnetic field. This amplitude can be then converted into an electric potential using an appropriate operator, such that the presented approach based on the Tikhonov regularization can be applied [33]. The airborne/seaborne surveying provides the

information on aquifers for groundwater investigations, paleochannels for shallow gas investigation and drilling hazards, on soils and overburden for engineering purposes [53,54]. Cloaking and illusion can be used in these studies as well, depending on purposes and needs of subsurface explorations.

The superposition principle in terms of active noise cancellation presented here can be used in other areas, e.g. in submarine engineering and marine research. The corrosion of a submarine may create an underwater electric potential that can be detected by available seabed mines with appropriated sensors [55]. The cancellation of the underwater electric potential could be improved by using the presented approach. Also, there are living creatures perceiving electric or electromagnetic signals, and this behaviour of the creatures is an important component of their survival strategy. For example, the Gnathonemus elephantfish, hammerhead shark and platypus rely on their electric receptors in muddy waters rather than on their optic sensory organs [56,57,58]. So, to hide objects from hammerhead sharks, a cloaking or deflecting device could be developed. We believe that an active cloaking and illusion in electrostatics will inspire new applications in geosciences, electrical engineering, live sciences, and elsewhere.

METHOD

We employ a weak formulation of the boundary value problem (equations 1 and 2) transforming it into an integral equation:

$$B(u,v) = L(f,v), \tag{9}$$

where the operators *B* and *L* are defined as $B(u,v) := \int_\Omega \sigma(x)\nabla u(x)\cdot\nabla v(x)\,dx + \int_{\partial\Omega} g(x)u(x)v(x)\,dS$ and $L(f,v) := -\int_\Omega f(x)v(x)dx$. Here v is the test function, and *S* is the boundary element. The solution to the problem (9) for given σ and f (the electric potential u) is the weak solution to the original problem [41,42] (equations 1 and 2). This solution is unique in the case of sufficiently smooth function σ [59].

We specify the model domain as a cuboid $\Omega = [0.0,\ 20.0]\times[0.0,\ 30.0]\times[-6.0,\ 2.0]$ with length unit km, where SSD is represented as $\Omega^l = [0.0,\ 20.0]\times[0.0,\ 30.0]\times[-6.0,\ 0.0]$, OSD as $\Omega^u = [0.0,\ 20.0]\times[0.0,\ 30.0]\times[0.0,\ 2.0]$, and ISD (or Σ) as $x_3 = 0$. The finite-element method

(FEM) is employed [42], and the model domain is discretized by tetrahedral finite elements at $n = 18 \times 10^3$ nodes. The electric potential u and the test function v are approximated by a combination of n linear finite elements, that is, piecewise linear polynomials, $\{v_i\}_{i=1}^{n}$, i.e. $u(x) := \sum_{i=1}^{n} u_i v_i(x)$ and $\mathbf{u} := (u_1, u_2, \ldots, u_n)^{\mathrm{T}} \in \mathbb{R}^n$. Inserting the approximation into equation (9), we obtain a discrete problem corresponding to the problem (9)

$$\mathbf{Bu} = \mathbf{Lf}\,, \tag{10}$$

valid for all v_i $(i = 1, 2, 3, \ldots, n)$ with matrices

$$\mathbf{B} := \left\{ B_{ij} = \int_\Omega \sigma(\mathbf{x}) \nabla v_i(\mathbf{x}) \cdot \nabla v_j(\mathbf{x})\, d\mathbf{x} + \int_{\partial\Omega} \mathrm{g}(\mathbf{x}) v_i(\mathbf{x}) v_j(\mathbf{x})\, dS \right\} \in \mathbb{R}^{n \times n},$$

$$\mathbf{L} := \left\{ L_{ij} = -\int_\Omega f_i(\mathbf{x}) v_j(\mathbf{x})\, d\mathbf{x} \right\} \in \mathbb{R}^{n \times n},\ (i, j = 1, 2, \ldots, n).$$ The vectors $\mathbf{u}$ and $\mathbf{f}$ are discrete representatives of the electric potential and the current source density, respectively. Sommer et al. [33] showed that the numerical direct problem (10) is well-posed, and the operator $\mathbf{B}$ is positive definite and invertible. Hence, the solution to (10) is $\mathbf{u} = \mathbf{B}^{-1}\mathbf{L}\,\mathbf{f} =: \mathbf{Af}$. It is important to note that the existence of the forward problem's solver operator $\mathbf{A} = \mathbf{B}^{-1}\mathbf{L}$ and its positive definition [41] as well as the symmetry and the positive definition of matrix $\mathbf{L}$ yield the operator $\mathbf{A}$ to be invertible.

At each node of the discrete model domain $\boldsymbol{\Omega}$, we assume the specific electrical conductivity to be $\sigma = 10^{-1}$ S (Siemens) m^{-1} for $x_3 \le 0$ (in the SSD and on the ISD), and $\sigma = 10^{-6}$ S m^{-1} for $x_3 > 0$ (in the OSD). We consider two examples of artificial current source densities (in A m^{-3}):

$$\mathbf{f}^{+}(\mathbf{x}) := \begin{cases} 4, & \mathbf{x} \in Q, \\ -1, & \mathbf{x} \in K \setminus \mathrm{Q}, \\ 0, & \text{elsewhere}, \end{cases} \qquad \mathbf{f}^{\square}(\mathbf{x}) := \begin{cases} 1, & x_2 \ge 0 \text{ and } \mathbf{x} \in R, \\ -1, & x_2 < 0 \text{ and } \mathbf{x} \in R, \\ 0, & \text{elsewhere}, \end{cases}$$

where

$$Q = [8.5,\ 11.5]\ \mathrm{km} \times [13.5,\ 16.5]\ \mathrm{km} \times [-3.5, -2.5]\ \mathrm{km},$$

$$K = (([8.5,\ 11.5]\ \mathrm{km} \times [10.5,\ 19.5]\ \mathrm{km}) \cup ([5.5,\ 14.5]\ \mathrm{km} \times [13.5,\ 16.5]\ \mathrm{km})) \times [-3.5, -2.5]\ \mathrm{km}'$$

352 $$R = (([6.0,\ 14.0]\ \text{km} \times [11.0,\ 19.0]\ \text{km}) \setminus ([8.0,\ 12.0]\ \text{km} \times [13.0,\ 17.0]\ \text{km})) \times [-3.5, -2.5]\ \text{km}.$$

353 Note that the support K of $\mathbf{f}^{+}$ is a simply connected domain (a "cross") and the support R of
354 $\mathbf{f}^{\square}$ is a double connected domain (a "ring"). Function *g* is defined in the model as
355 $g(\mathbf{x}) = \left(\left[x_1 - 10\ (\text{km}) \right]^2 + \left[x_2 - 15\ (\text{km}) \right]^2 + \left[x_3 + 2\ (\text{km}) \right]^2 \right)^{-1/2}$.

356 We employ the COMSOL Multiphysics FEM software (www.comsol.com) to generate the
357 mesh. The direct and the inverse problem solvers are implemented in MATLAB
358 (www.mathworks.com), which is linked to COMSOL Multiphysics.

359 In constructing the cloaking device, we assume that the complementary current source
360 density $\mathbf{f}_c$ has a support on the ISD, and introduce a continuation operator $\mathbf{U}$ extending the
361 support as $\mathbf{U}\mathbf{f}_c(\mathbf{x}) = \mathbf{f}_c(\mathbf{x}),\ \mathbf{x} \in \Sigma$, and 0 elsewhere in $\boldsymbol{\Omega}$. Thus, the domain of the cloaking device
362 corresponds to the domain of $\mathbf{f}_c$ and is shaped by $\mathbf{U}$. We introduce the adapted operator, which
363 maps the cloaking current source density to the electrical potential in the entire domain Ω:
364 $\mathbf{A}_{d,c} := \mathbf{A}_d \mathbf{U}$. The active cloaking problem is formulated as a minimization problem with a
365 penalty term:

366 $$\frac{1}{2} \left\| \mathbf{A}_{d,c} \mathbf{f}_c(\mathbf{x}) + \mathbf{u}_d(\mathbf{x}) \right\|^2_{L_2(\Gamma)} + \frac{\alpha}{2} \left\| \mathbf{D}\mathbf{f}_c(\mathbf{x}) \right\|^2_{L_2(\Sigma)} \ \rightarrow \ \min_{\mathbf{f}_c}, \tag{11}$$

367 where $L_2(G)$ is the space of functions that are square integrable over domain G, equipped
368 with the standard scalar product $(\mathbf{u}, \mathbf{v}) = \int_G \mathbf{u}(\mathbf{x})\mathbf{v}(\mathbf{x}) dG$ and the norm $\|\mathbf{v}\| = (\mathbf{v}, \mathbf{v})^{1/2}$. The
369 solution to the minimization problem (11) can be found using the Tikhonov regularization in the
370 following form [60]:

371 $$\mathbf{f}_{c,\alpha} = -\boldsymbol{\Lambda}_{c,\alpha} \mathbf{u}_d, \tag{12}$$

372 where $\boldsymbol{\Lambda}_{c,\alpha} = (\mathbf{A}^{\mathrm{T}}_{d,c} \mathbf{A}_{d,c} + \alpha \mathbf{D}^{\mathrm{T}} \mathbf{D})^{-1} \mathbf{A}^{\mathrm{T}}_{d,c}$ is the cloaking operator, and $\mathbf{f}_{c,\alpha}$ is the current source
373 density of the cloaking device. We define here the electric potential data on Γ generated by
374 $\mathbf{f}_{c,\alpha}$ as

375 $$\mathbf{u}_{d,c} := \mathbf{A}_{d,c} \mathbf{f}_{c,\alpha} \approx -\mathbf{u}_d. \tag{13}$$

The cloaking procedure (7) can be then obtained using equations (12) and (13).

Data availability. The codes and datasets generated during the current study are available from the first author on a request.

REFERENCES

[1] Alu, A. & Engheta, N. Achieving transparency with plasmonic and metamaterial coatings. *Phys. Rev. E* **72**, 016623; https://doi.org/10.1103/PhysRevE.72.016623 (2005).

[2] Schurig, D., Mock, J., Justice, B., Cummer, S., Pendry, J., Starr, A. & Smith, D. Metamaterial electromagnetic cloak at microwave frequencies, *Science* **314**, 977-980 (2006).

[3] Ang, P. & Eleftheriades, G.V. Active cloaking of a non-uniform scatterer. *Sci. Rep.* **10**, 2021; https://doi.org/10.1038/s41598-020-58706-z (2020).

[4] Torrent, D. & Sanchez-Dehesa, J. Acoustic cloaking in two dimensions: a feasible approach, *New J. Phys.***10**, 063015; https://doi.org/10.1088/1367-2630/10/6/063015 (2008).

[5] Chen, H. & Chan, C.T. Topical Review - Acoustic cloaking and transformation acoustics, *J. Phys. D: Appl. Phys.* **43**, 113001; https://doi.org/10.1088/0022-3727/43/11/113001 (2010).

[6] Ryoo, H. & Jeon, W. Effect of compressibility and non-uniformity in flow on the scattering pattern of acoustic cloak. *Sci. Rep.* **7,** 2125; https://doi.org/10.1038/s41598-017-02143-y (2017).

[7] Guenneau, S., Amra, C. & Veynante, D. Transformation thermodynamics: cloaking and concentrating heat flux, *Optics Express* **20**(7), 8207–8218 (2012).

[8] Leonhard, U. Cloaking of heat, *Nature* **498**, 440-441 (2013).

[9] Stedman, T. & Woods, L.M. Cloaking of thermoelectric transport. *Sci. Rep.* **7,** 6988: https://doi.org/10.1038/s41598-017-05593-6 (2017).

[10] Imran, M., Zhang, L. & Gain, A.K. Advanced thermal metamaterial design for temperature control at the cloaked region. *Sci. Rep.* **10,** 11763; https://doi.org/10.1038/s41598-020-68481-6 (2020).

[11] Bückmann, T., Thiel, M., Kadic, M., Schittny, R. & Wegener, M. An elasto-mechanical unfeelability cloak made of pentamode metamaterials, *Nat. Comm.* **5**, 4130; https://doi.org/10.1038/ncomms5130 (2014).

[12] Brun, M., Guenneau, S. & Movchan, A. B. Achieving control of in-plane elastic waves, *App. Phys. Lett.* **94**, 061903; https://doi.org/10.1063/1.3068491 (2009).

[13] Norris, A.N. & Shuvalov, A.L. Elastic cloaking theory, *Wave Motion* **48**(6), 525-538 (2011).

[14] Stenger, N., Wilhelm, M. & Wegener M.. Experiments on elastic cloaking in thin plates, *Phys. Rev. Lett.* **108,** 014301; https://doi.org/10.1103/PhysRevLett.108.014301 (2012).

[15] Lee, M. & Kim, Y. Add-on unidirectional elastic metamaterial plate cloak. *Sci. Rep*. **6,** 20731: https://doi.org/10.1038/srep20731 (2016).

[16] Kim, S.-H. & Das, M.P. Seismic waveguide of metamaterials, *Mod. Phys. Lett. B* **26**, 1250105(8): https://doi.org/10.1142/S0217984912501059 (2012).

[17] Brûlé, S., Javelaud, E.H., Enoch, S. & Guenneau, S. Experiments on seismic metamaterials: molding surface waves, *Phys. Rev. Lett.* **112**, 133901(5); https://doi.org/10.1103/PhysRevLett.112.133901 (2014).

[18] Colombi, A., Colquitt, D., Roux, P., Guenneau, S. & Craster, R. A seismic metamaterial: The resonant metawedge, *Sci. Rep.* **6**, 27717; https://doi.org/10.1038/srep27717 (2016).

[19] Lott, M., Roux, P., Garambois, S, Guéguen, P., & Colombi, A. Evidence of metamaterial physics at the geophysics scale: the METAFORET experiment, *Geophys. J. Int.* **220**, 1330–1339 (2020).

[20] Norris, A.N., Amirkulova, F.A & Parnell, W.J. Source amplitudes for active exterior cloaking, *Inv. Prob.* **28**, 105002: https://doi.org/10.1088/0266-5611/28/10/105002 (2012).

[21] Li, J. & Pendry, J.B. Hiding under the carpet: A new strategy for cloaking, *Phys. Rev. Lett.* **101**, 203901: https://doi.org/10.1103/PhysRevLett.101.203901 (2008).

[22] Liu, R., Ji, C., Mock, J.J., Chin, J. Y., Cui T.J. & Smith, D.R. Broadband ground-plane cloak, *Science* **323**, 366–369 (2009).

[23] Cai, W. & Shalaev, V. *Optical Metamaterials – Fundamentals and Applications*, Springer-Verlag New York (2010).

[24] Ergin, T., Stenger, N., Brenner, P., Pendry, J.B. & Wegener, M. Three-dimensional invisibility cloak at optical wavelengths, *Science* **328**, 337-339 (2010).

[25] Chen, X. & Uhlmann, G. Cloaking a sensor for three-dimensional Maxwell's equations: transformation optics approach, *Optics Express* **19**(21), 20518-20530 (2011).

[26] Greenleaf, A., Kurylev, Y., Lassas, M. & Uhlmann, G. Cloaking devices, electromagnetic wormholes, and transformation optics, *SIAM Rev.* **51**(1), 3–33 (2009).

[27] Vasquez, F.G., Milton, G.W. & Onofrei, D. Active exterior cloaking for the 2D Laplace and Helmholtz equations, *Phys. Rev. Lett.* **103**, 073901; https://doi.org/10.1103/PhysRevLett.103.073901 (2009).

[28] Sanchez, A., Navau, C., Prat-Camps, J. & Chen, D.-X. Antimagnets: controlling magnetic fields with superconductor-metamaterial hybrids, *New J. Phys*. **13**, 093034: https://doi.org/10.1088/1367-2630/13/9/093034 (2011).

[29] Selvanayagam, M. & Eleftheriades, G.V. Discontinuous electromagnetic fields using orthogonal electric and magnetic currents for wavefront manipulation, *Opt. Express* **21**, 14409-14429 (2013).

[30] Tikhonov, A.N. Solution of incorrectly formulated problems and the regularization method. *Doklady Akademii Nauk SSSR*, **151**, 501–504. Engl. transl.: *Soviet Mathematics Doklady* **4**, 1035–1038 (1963).

[31] Snyder, S.D. *Active Noise Control Primer - Modern Acoustics and Signal Processing*. Springer, New

York (2000).

[32] Cheer, J. Active control of scattered acoustic fields: Cancellation, reproduction and cloaking, *J. Acoust. Soc. Am.* **140**(3), 1502-1512 (2016).

[33] Sommer, A., Helfrich-Schkarbanenko, A. & Heuveline, V. Identification of current sources in 3D electrostatics. In: *Handbook of Geomathematics*, W. Freeden, M. Z. Nashed, and T. Sonar (eds.) Berlin-Heidelberg: Springer-Verlag, pp. 1-19 (2014).

[34] Saracco, G., Labazuy, Ph. & Moreau, F. Localization of self-potentials in volcano-electric effect with complex continuous wavelet transform and electrical tomography methods for an active volcano, *Geophys. Res. Lett*. **31**(12); https://doi.org/10.1029/2004GL019554 (2004).

[35] Brothlande, E., Finizola, A., Peltier, A., Delcher, E., Komorowski, J.,-C., Di Gangi, F., et al. Fluid circulation pattern inside La Soufrière volcano (Guadeloupe) inferred from combined electrical resistivity tomography, self-potential, soil temperature and diffuse degassing measurements, *J. Volcanol. Geother. Res.* **288**, 105-122 (2014).

[36] Kawada, Y. & Kasaya, T. Marine self-potential survey for exploring seafloor hydrothermal ore deposits. *Sci. Rep.* **7,** 13552; https://doi.org/10.1038/s41598-017-13920-0 (2017).

[37] Lai, Y., Ng, J., Chen, H., Han, D., Xiao, J., Zhang, Z.-Q. & Chan, C. Illusion optics: the optical transformation of an object into another object, *Phys. Rev. Lett.* **102**, 253902: https://doi.org/10.1103/PhysRevLett.102.253902 (2009).

[38] Vandemeulebrouck, J., Roux, P., Gouedard, P., Legaz, A., Revil, A., Hurst, A.W., Boleve, A. & Jardani, A. Application of acoustic noise and self-potential localization techniques to a buried hydrothermal vent (Waimangu Old Geyser site, New Zealand), *Geophys. J. Int.* **180**, 883–890 (2010).

[39] Bédard, C. & Destexhe, A. Generalized theory for current-source-density analysis in brain tissue, *Phys. Rev. E* **84**, 041909; https://doi.org/10.1103/PhysRevE.84.041909 (2011).

[40] Akin, J. E.. *Finite Element Analysis with Error Estimators: An Introduction to the FEM and Adaptive Error Analysis for Engineering Students*, Elsevier (2005).

[41] Brenner, S.C. & Scott, L.R. *The Mathematical Theory of Finite Element Methods*. New York: Springer (1994).

[42] Ismail-Zadeh, A. & Tackley P.J. *Computational Methods for Geodynamics*, Cambridge University Press, Cambridge (2010).

[43] Zhdanov, M.S. *Geophysical Inverse Theory and Regularization Problems*. Elsevier, Amsterdam (2002).

[44] Hansen, P. *Rank-Deficient and Discrete Ill-Posed Problems: Numerical Aspects of Linear Inversion.* Philadelphia: SIAM (1998).

[45] Zlotnicki, J. Sasai, Y., Yvetot, P., Nishida, Y., Uyeshima, M., Fauquet, F., Utada, H., Takahashi, Y. & Donnadieu, G. Resistivity and self-potential changes associated with volcanicactivity: The July 8,

480 2000 Miyake-jima eruption (Japan), *Earth Planet. Sci. Lett.* **205**, 139–154 (2003).
481 [46] Pride, S.R. Governing equations for the coupled electromagnetics and acoustics of porous media,
482 *Phys Rev B* **50**, 15678–15696 (1994).
483 [47] Jouniaux, L. & Zyserman, F. A review on electrokinetically induced seismo-electrics, electro-seismics,
484 and seismo-magnetics for Earth sciences, *Solid Earth* **7**, 249–284 (2016).
485 [48] Schlumberger, C., Schlumberger, M. & Leonardon, E. G. A new contribution to subsurface studies
486 by means of electrical measurements in drill holes, *AIME Transactions* **110**(1), 273-288 (1934).
487 [49] Lénat, J. F. Geoelectrical methods in volcano monitoring. In: *Monitoring active volcanoes*, B. M
488 Guire, C. Kilburn & J. Murray (eds.), UCL Press, London, pp. 248-274 (1995).
489 [50] Martínez-Pagán, P., Jardani, A., Revil, A. & Haas, A. Self-potential monitoring of a salt plume,
490 *Geophysics* **75**(4), WA17-WA25 (2010).
491 [51] Haas, A. K., Revil, A., Karaoulis, M., Frash, L., Hampton, J., Gutierrez, M. & Mooney, M. Electric
492 potential source localization reveals a borehole leak during hydraulic fracturing, *Geophysics* **78**(2),
493 D93-D113 (2013).
494 [52] Revil, A. & Jardani, A. *The Self-Potential Method: Theory and Applications in Environmental*
495 *Geosciences*, Cambridge University Press, Cambridge (2013).
496 [53] Sengpiel, K.-P. & Siemon, B. Advanced inversion methods for airborne electromagnetic exploration,
497 *Geophysics* **65**, 1983–1992 (2000).
498 [54] Siemon, B. Electromagnetic methods – frequency domain: Airborne techniques, in Kirsch, R. (ed.),
499 *Groundwater Geophysics – A Tool for Hydrogeology*, 2nd ed., Springer, Berlin, pp. 155–170 (2009).
500 [55] Schäfer, D., Doose, J., Rennings, A. & Erni, D. Numerical analysis of propeller-induced low-frequency
501 modulations in underwater electric potential signatures of naval vessels in the context of corrosion
502 protection systems. In: Proc. of the COMSOL Conference Stuttgart, Germany, 26-28 October (2011).
503 [56] Heiligenberg, W. *Principles of Electrolocation and Jamming Avoidance in Electric Fish: A*
504 *Neuroethological Approach*. Springer, Berlin (1977).
505 [57] Scheich, H., Langner, G., Tidemann, C., Coles, R. B. & Guppy, A. Electroreception and electrolocation
506 in platypus, *Nature* **319**, 401–402 (1986).
507 [58] Kajiura, S. M. & Holland, K.N. Electroreception in juvenile scalloped hammerhead and sandbar
508 sharks, *J. Exper. Biol.* **205**, 3609-3621 (2002).
509 [59] Gilbarg, D. & Trudinger, N.S. *Elliptic Partial Differential Equations of Second Order*, 2nd ed., Springer,
510 Berlin (1989).
511 [60] Helfrich-Schkarbanenko, A. Elektrische Impedanztomografie in der Geoelektrik: Das Unzugängliche
512 erforschen, Dissertation, Karlsruher Institut für Technologie (2011).
513
514

Acknowledgments. AIZ acknowledges a support from the Russian Science Foundation (RSF-19-17-00027).

Authors' contribution. AHS and AIZ conceived the research, stated the problems and analysed the results. AHS and AS designed cloaking and illusion devices and conducted numerical experiments; AIZ and AHS wrote the manuscript and prepared figures, and all authors reviewed the manuscript.

Competing interest. The authors declare no competing interests.

Figures

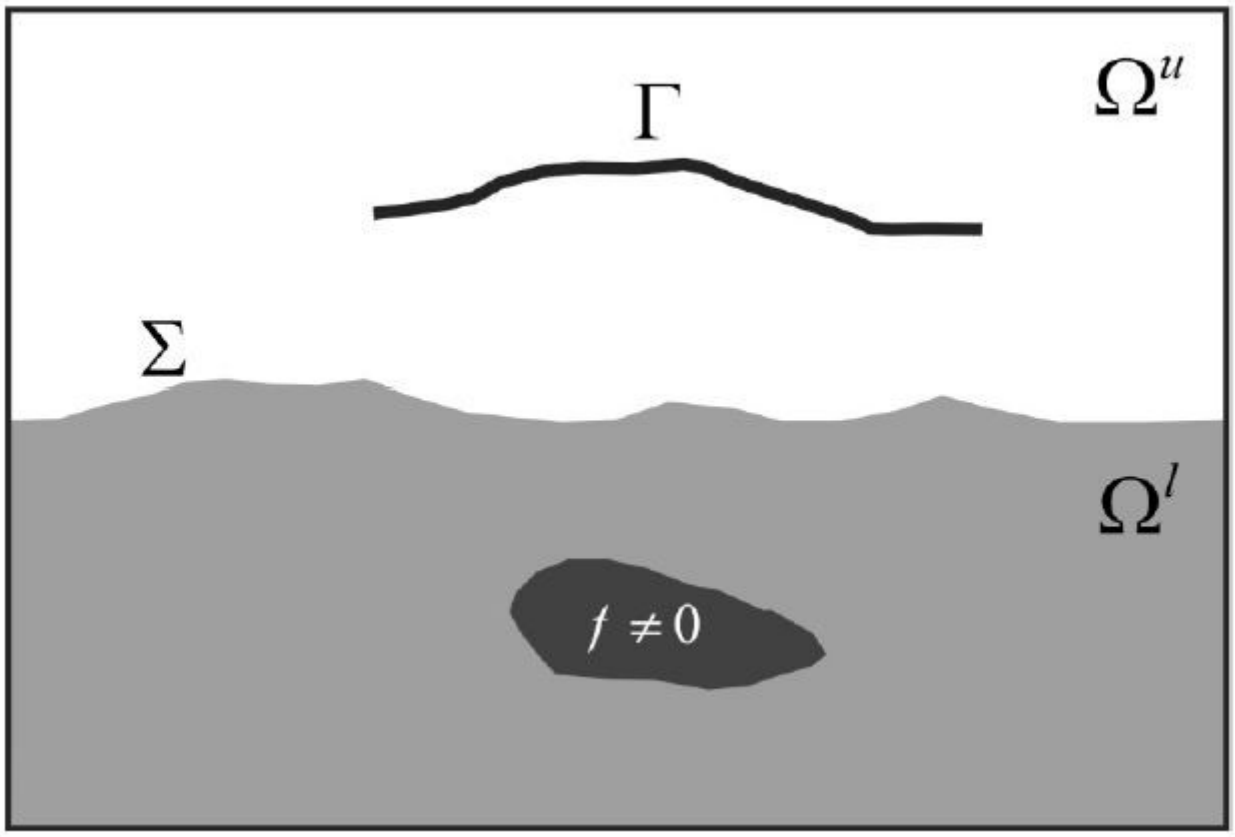

Figure 1

Two-dimensional cartoon of the model domain Ω. Dark gray: the area of non-zero current source density; light gray: the SSD lΩ; Σ is the lSD; uΩ is the OSD; and Γ is a curve (or a set) of measurement points.

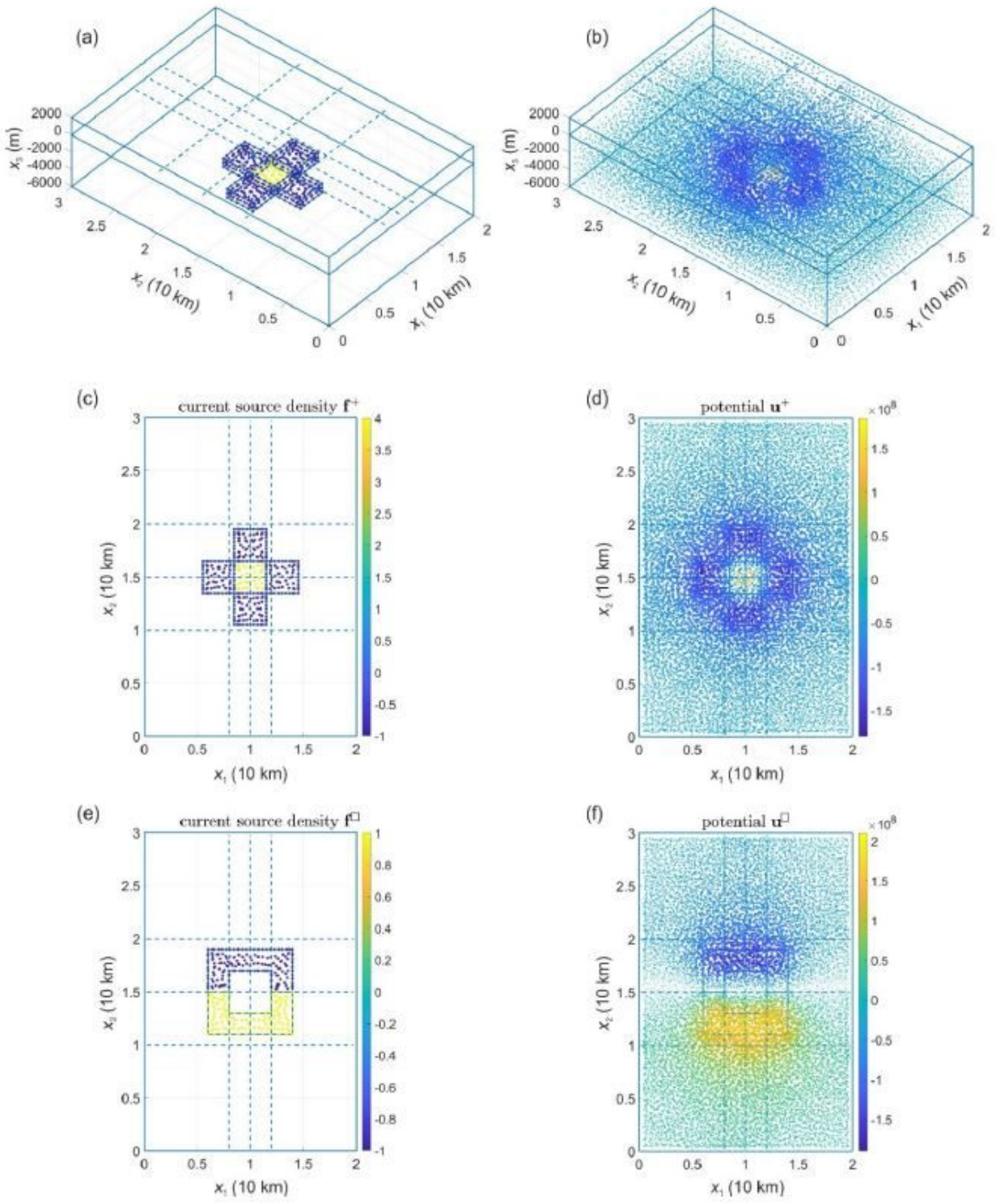

Figure 2

Electric potentials generated by two current source densities. The perspective view (a) and top 118 view (c) of the current source density +f; the perspective view (b) and top view (d) of the electric 119 potential +u generated by the current source density. Top view of the electric potential u+ (f) 120 generated by f+ (e). Here and in Figs. 3-6, a top view image presents a transparent projection of 121 physical quantities at finite element nodes on the plane. The size of the nodes in the images is 122 proportional to the absolute

value of the physical quantities it represents, i.e. the nodes with zero-values 123 are not displayed. Dashed lines show the position of the paths, along which synthetic measurements of 124 the electric potential have been made.

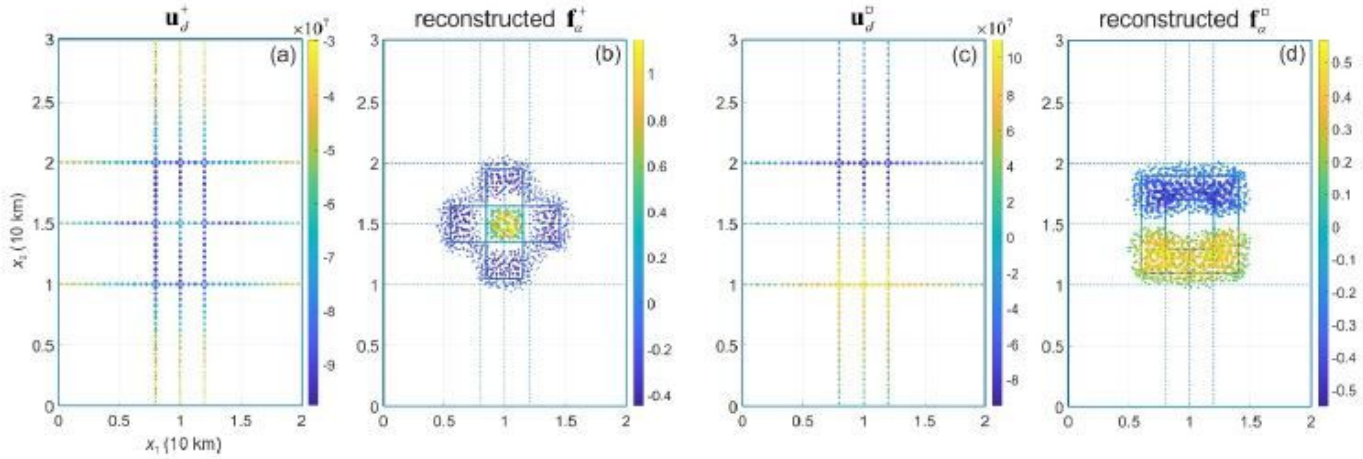

Figure 3

Electric potential d+u (a) and du+ (c) along the paths of synthetic measurements, and the current source density α+f (b) and αf+ (d) reconstructed from the synthetic measured data.

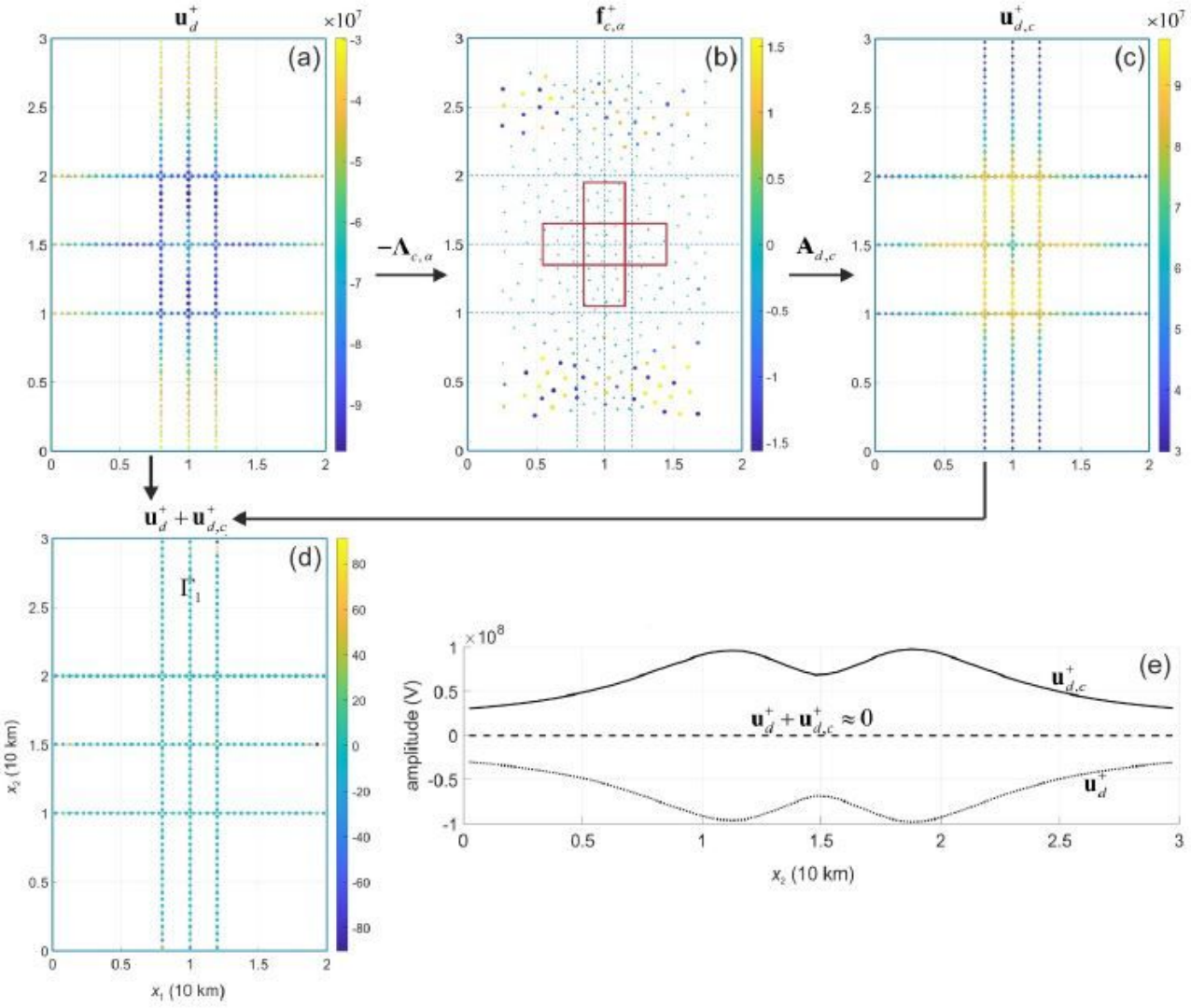

Figure 4

Active cloaking of the electric potential d+u on Γ (a) generated by the current source density +f. Using equation (13) the cloaking devise is modelled by the current source density ,cα+f (b) that generates ,dc+u (c) leading to a significant reduction (almost cancellation) of the electric potential signal on Γ (d). Panel (e) demonstrates the cancellation of the signal ,ddc+++uu (see dashed line) on the middle path (line 1Γ: 13:0 km; 0.5 km{}uxx□Ω==□xΓ) of the synthetic measurement data.

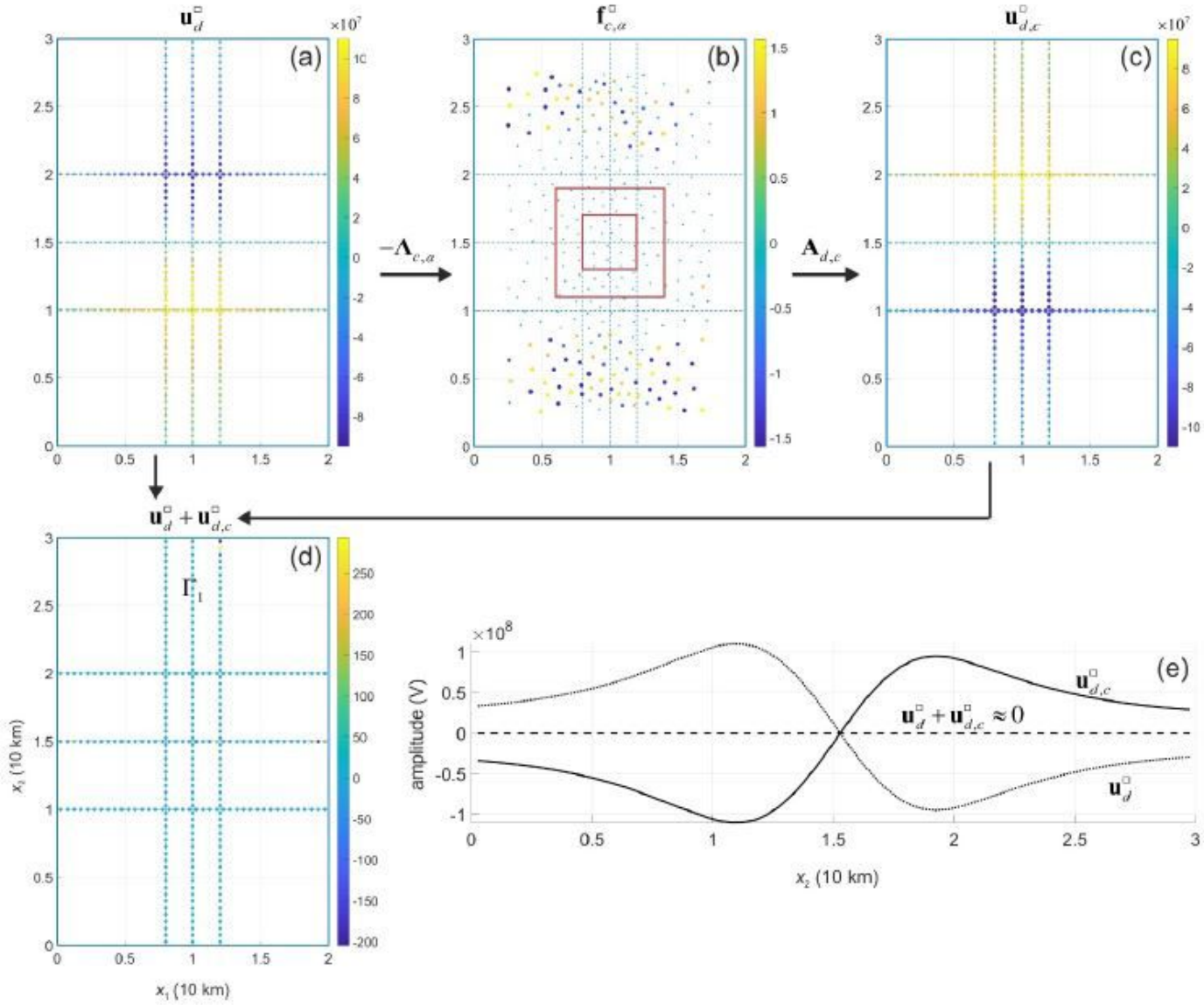

Figure 5

Active cloaking of the electric self-potential du+ on Γ (a) generated by the current source density f+. Using equation (13) the cloaking devise is modelled by the current source density ,cαf+ (b) that 216 generates ,dcu+ (c) leading to a significant reduction (almost cancellation) of the electric potential signal 217 on Γ (d). Panel (e) demonstrates the cancellation of the signal ,ddc+uu+ (see dashed line) on line 1Γ 218 13:0 km; 0.5 km{}Ω==axxxΓ.

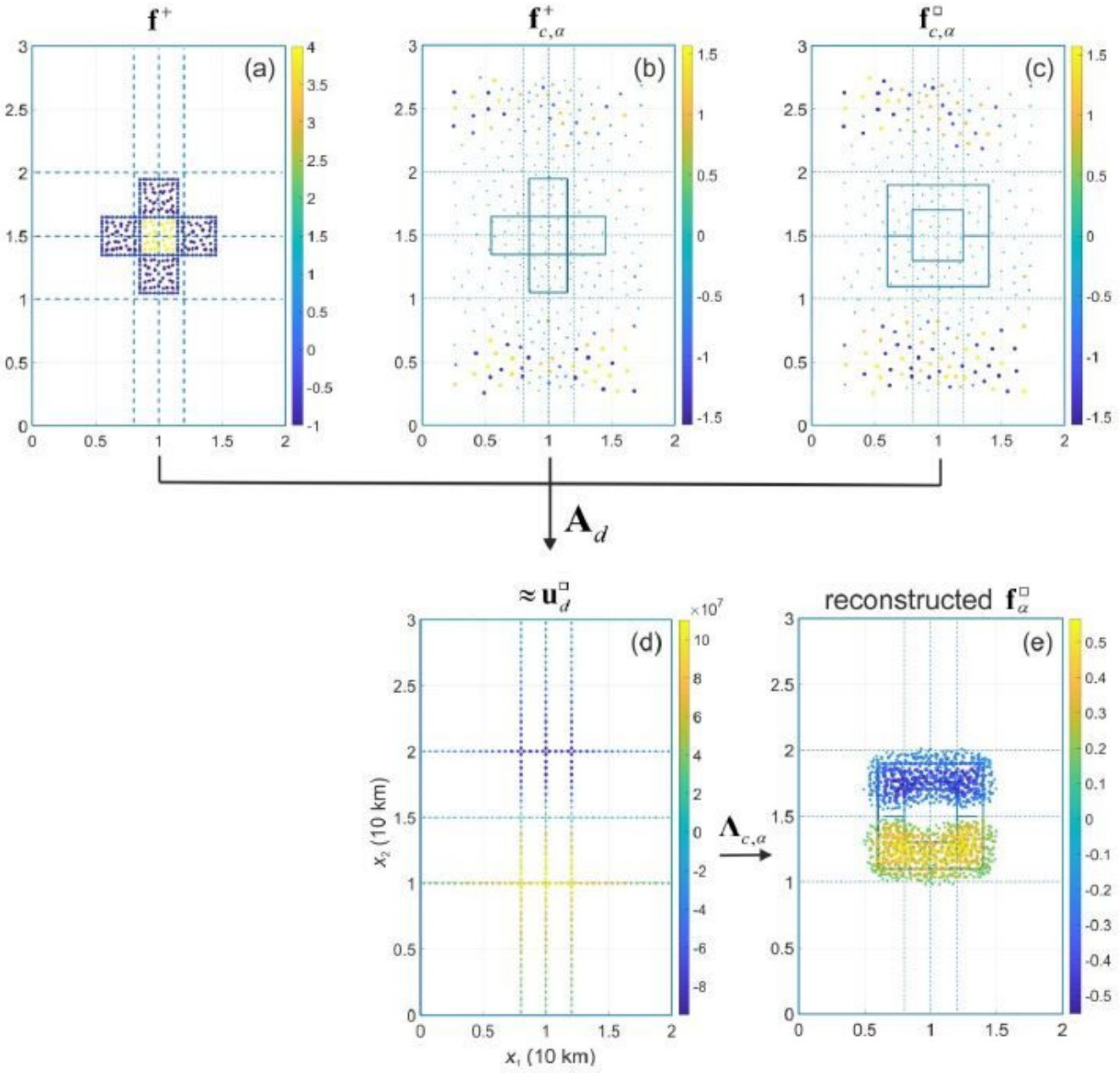

Figure 6

Illusion of the current source density f+ by cloaking of the current source density +f (a) using cloaking devices ,cα+f (b) and ,cαf+ (c). Panel (d) represents a composition data on electric potential, which will be measured in the case of illusion (equation 16), and panel (e) illustrates the reconstruction of current source density from these measured data.

Supplementary Files

This is a list of supplementary files associated with this preprint. Click to download.

- SuppMaterA3SciRep.pdf